RESEARCH ARTICLE | MAY 08 2025

# Structural, elastic, electronic, thermoelectric, and thermodynamic properties of cubic $LaMgX_2$(X=Cd, Zn, Hg): For sustainable technologies

A. Benamrani ; M. A. Ghebouli ; B. Ghebouli; M. Fatmi ; Razan A. Alshgari; Saikh Mohammad; Mika Sillanpää



*AIP Advances* 15, 055109 (2025)
https://doi.org/10.1063/5.0269533

# Structural, elastic, electronic, thermoelectric, and thermodynamic properties of cubic $LaMgX_2$ (X=Cd, Zn, Hg): For sustainable technologies

Cite as: AIP Advances 15, 055109 (2025); doi: 10.1063/5.0269533
Submitted: 6 March 2025 • Accepted: 28 April 2025 •
Published Online: 8 May 2025



A. Benamrani,[1] M. A. Ghebouli,[2,3] B. Ghebouli,[4] M. Fatmi,[2,a)] Razan A. Alshgari,[5] Saikh Mohammad,[5] and Mika Sillanpää[6,7]

## AFFILIATIONS

[1] Laboratory of Materials Physics, Radiation and Nanostructure (LPMRN), University Mohamed El Bachir El Ibrahimi of Bordj Bou Arreridj, 34000 Bordj Bou Arreridj, Algeria
[2] Research Unit on Emerging Materials (RUEM), University of Setif 1, 19000 Setif, Algeria
[3] Department of Chemistry, Faculty of Sciences, University of M'sila University Pole, Road Bourdj Bou Arreiridj, 28000 M'sila, Algeria
[4] Laboratory of Studies Surfaces and Interfaces of Solids Materials, Department of Physics, Faculty of Science, University Ferhat Abbas of Setif 1, 19000 Setif, Algeria
[5] Department of Chemistry, College of Science, King Saud University, Riyadh 11451, Saudi Arabia
[6] Department of Biological and Chemical Engineering, Aarhus University, Norrebrogade 44, 8000 Aarhus C, Denmark
[7] Saveetha School of Engineering, Saveetha Institute of Medical and Technical Sciences, Saveetha University, Chennai, Tamil Nadu 602105, India

[a)] **Author to whom correspondence should be addressed:** Fatmimessaoud@yahoo.fr

## ABSTRACT

In this study, we investigate the structural, elastic, electronic, and thermodynamic properties of $LaMgX_2$ (X = Zn, Cd, Hg) intermetallic hydrides using first-principle calculations based on density functional theory. The compounds exhibit metallic behavior with relatively high bulk moduli, suggesting good mechanical stability. The thermodynamic parameters, such as Debye temperature and entropy, were derived and analyzed to evaluate their thermal stability. Furthermore, the hydrogen storage potential of these compounds was assessed, revealing favorable characteristics for reversible hydrogen absorption and desorption. In addition, their thermoelectric properties were investigated by evaluating key indicators such as the Seebeck coefficient, electrical conductivity, and the electronic contribution to thermal conductivity. These insights into energy transport behavior further support their multifunctional potential. Overall, these findings highlight the potential of $LaMgM_2$ hydrides as promising candidates for hydrogen storage applications, especially in energy-efficient technologies.



## I. INTRODUCTION

The intermetallic compounds characterized by the general formula $LaMgX_2$ (where X represents Cd, Zn, or Hg) have attracted significant research interest for their dual potential as hydrogen storage media and lightweight structural components. Among these, the cadmium-containing variant $LaMgCd_2$ exhibits particularly favorable characteristics, including reduced mass density, superior thermal resistance, and excellent machining properties. These attributes, combined with the hydrogen absorption capabilities inherent to magnesium, establish $LaMgCd_2$ as a promising candidate for hydrogen storage systems and various industrial applications.[1,2] Comparative analyses reveal that these alloys demonstrate enhanced hydrogen absorption and desorption kinetics when compared to pure magnesium. The $LaMgX_2$ intermetallic compounds possess distinctive physicochemical profiles that

differentiate them substantially from conventional metal alloys. For instance, incorporating zinc into the magnesium–lanthanum system significantly enhances both ductility and mechanical resistance, rendering $LaMgZn_2$ particularly valuable in aerospace engineering, automotive manufacturing, and structural frameworks.[3,4] In addition, zinc inclusion in this intermetallic system contributes to superior resistance against localized corrosive processes, making $LaMgZn_2$ particularly well-suited for deployment under aggressive environmental conditions. Substituting mercury (Hg) in the system modifies the electronic behavior of the resulting compound, although widespread industrial implementation remains constrained by mercury's toxicological profile.[5] Nevertheless, the unique electronic characteristics of $LaMgHg_2$ render it particularly applicable for sensing technologies and specialized electronic instrumentation. Magnesium has been extensively documented for its capacity to absorb and store hydrogen. The $LaMgX_2$ systems (X = Cd, Zn, Hg) enhance this capacity while simultaneously improving thermodynamic stability and absorption kinetics, resulting in more efficient hydrogen storage solutions.[6] The remarkable stability exhibited by these intermetallic compounds substantially augments their hydrogen storage capacity a critical feature for applications in fuel cell technologies and hydrogen-powered transportation systems. Research conducted by Züttel and colleagues examines magnesium alloys enhanced with rare earth elements, particularly lanthanum, which demonstrate considerable potential for forming stable hydride compounds, thereby enhancing hydrogen storage characteristics.[7] The lanthanum component establishes conditions conducive to hydrogen interaction, consequently increasing absorption capacity. Investigations by Sato and Yartys explore the hydrogen storage potential of $LaMg_2$ and LaMgNi(4−x)Co(x) intermetallic systems.[8] These alloys maintain structural integrity at elevated temperatures, making them appropriate for thermally demanding environments. The LaMgNi(4−x)Co(x) series demonstrates particularly efficient hydrogen storage capabilities, achieving absorption capacities between 1.5 and 2.0 weight percent hydrogen, positioning them as ideal candidates for hydrogen storage applications. Their research underscores the importance of optimizing both processing methodologies and compositional parameters to achieve performance characteristics required for practical energy storage implementations. In conclusion, continued exploration of the $LaMgX_2$ (X = Cd, Zn, Hg) alloy systems represent a promising direction toward developing advanced materials for sustainable energy storage and lightweight structural applications, addressing growing market demands for environmentally compatible technologies.

## II. CALCULATION METHOD

We calculated properties of $LaMgX_2$ (X = Cd, Hg, Zn) compounds using the Quantum Espresso software package[9] within the density functional theory (DFT) framework. For accurate exchange–correlation effects, we employed SG15 Optimized Norm-Conserving Vanderbilt pseudopotentials[10] and the Generalized Gradient Approximation (GGA) with the Perdew–Burke–Ernzerhof functional.[11] We set the plane wave cutoff energy at 110 Ry, which achieved our convergence criteria of $1 \times 10^{-4}$ Ry for energy and residual forces less than $1 \times 10^{-5}$ Ry/Bohr, balancing computational efficiency with accuracy. Brillouin zone integration utilized an $8 \times 8 \times 8$ Monkhorst–Pack k-point grid,[12] ensuring thorough electronic structure sampling. We employed the thermos-pw module[13] integrated with Quantum Espresso to calculate elastic stiffness constants and thermodynamic properties including vibrational energy, free energy, entropy, and constant-volume heat capacity. This module provided accurate temperature-dependent calculations essential for evaluating the stability and exploring potential applications of these intermetallic compounds for hydrogen storage systems and lightweight structural components.

## III. RESULTS AND DISCUSSION

### A. Crystal structure and stability

The intermetallic compounds $LaMgX_2$ (X = Cd, Hg, Zn) crystallize in the fluorite-type cubic structure with space group Fm-3m (No. 225). Within this structure, lanthanum (La) atoms form a face-centered cubic sublattice at the 4a (0, 0, 0) positions. Magnesium (Mg) atoms occupy the tetrahedral sites at the 4b (1/2, 1/2, 1/2) positions, while the X atoms (cadmium, mercury, or zinc) are situated at the octahedral sites, corresponding to the 8c (1/4, 1/4, 1/4) positions. The crystal structure of these $LaMgX_2$ compounds, clearly showing the atomic arrangements, is depicted in Fig. 1. The red, green, and blue balls represent the X, Mg, and La atoms, respectively. Figure 2 shows energy vs volume optimization curve for $LaMgX_2$(X = Cd, Zn, Hg). By comparing the curves that illustrate the relationship between the total energy and the volume of intermetallic LaMgHg2, LaMgZn2, and LaMgCd2, we see stability in the volumetric properties of these materials. $LaMgX_2$(X = Hg, Cd) compounds reach their lowest total energy 10 793.13 and 10 808.465 eV at a larger volume 103 and 104 $(Å)^3$ to achieve optimal stability. In addition, the energy curve has a steep slope; therefore, this total energy is more sensitive to changes in volume. In contrast, the lowest energy point for $LaMgZn_2$ 13 242.785 eV occurs at a slightly smaller volume of 89.5 $Å^3$. The curve for $LaMgZn_2$ exhibits a gentler slope, indicating greater stability against volumetric changes compared to $LaMgHg_2$ and $LaMgCd_2$. The pronounced energy drop at the stable volume indicates that $LaMgCd_2$ maintains high stability at reduced volumes, rendering it more resistant to volume

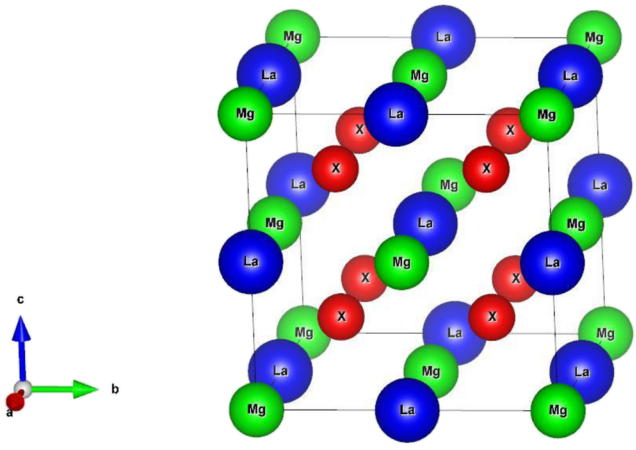


**FIG. 1.** Crystalline structure of $LaMgX_2$ (X = Zn, Cd, Hg).

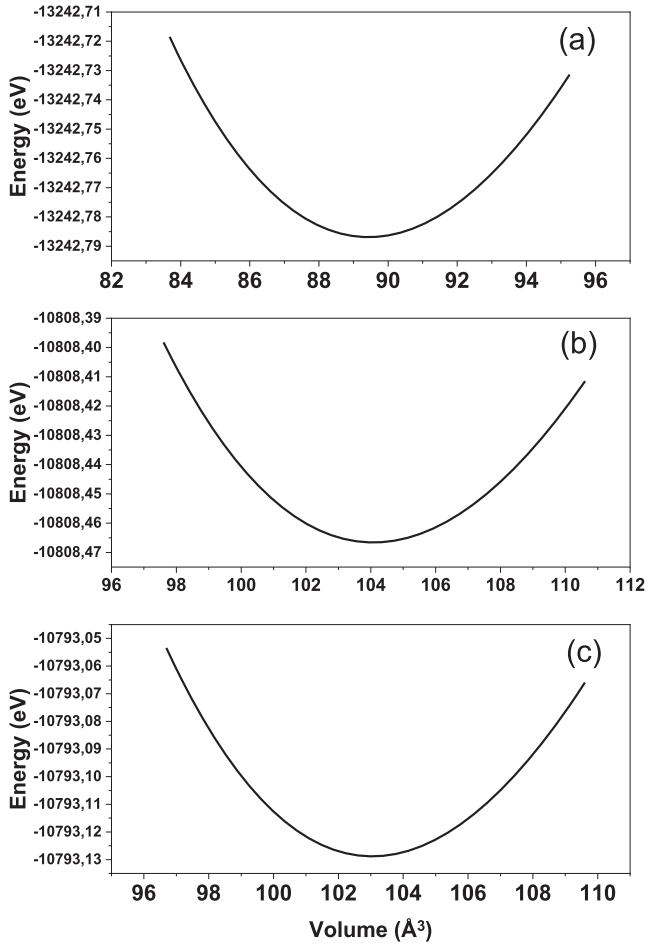


**FIG. 2.** Energy vs volume optimization curve of $LaMgZn_2$ (a), $LaMgCd_2$ (b), and (c) $LaMgHg_2$.

fluctuations. Table I presents our calculated equilibrium lattice constants ($a_0$), bulk moduli ($B_0$), and pressure derivatives of bulk moduli ($B_0$') for $LaMgZn_2$, $LaMgCd_2$, and $LaMgHg_2$, alongside existing experimental and theoretical values from the literature. The experimentally determined lattice constants are 7.05–7.10 Å for $LaMgZn_2$, 7.45 Å for $LaMgCd_2$, and 7.42 Å for $LaMgHg_2$,[14–16] with relative uncertainties less than 0.1%. These values align well with our computational results. Additional calculations using various density functional theory (DFT) implementations and alternative software packages have yielded comparable values, as documented in Refs. 15 and 16 for all three compounds. For $LaMgCd_2$ specifically, the experimental lattice constant of ~7.45 Å[16] closely matches our theoretical prediction, showing only minor deviations from values reported in Refs. 17–19. The strong agreement between our results and those obtained through different computational methods reinforces the reliability of this research. The consistency between calculated lattice constants and experimental measurements, together with the derived bulk moduli and pressure derivatives, suggests favorable elastic characteristics for these intermetallic compounds. Several

**TABLE I.** Lattice constant $a_0$ in (Å), $B$, B′ (GPa) of $LaMgZn_2$, $LaMgCd_2$, and $LaMgHg_2$.

| Compound | $a_0$ (Å) | $B$ (GPa) | $B'$ |
|---|---|---|---|
| $LaMgZn_2$ | 7.09 Exp. 7.05–7.10[14] | 52.52 | 4.30 |
| $LaMgCd_2$ | 7.46 Exp. 7.45[15] | 48.15 | 4.58 |
| $LaMgHg_2$ | 7.44 Exp. 7.42[16] | 54.31 | 4.87 |

structurally related intermetallic compounds have been reported in the literature, which support the feasibility of forming $LaMgM_2$-type hydrides. For instance, $La_2MgZn_2$ exhibits lattice constants in the range of 7.12–7.15 Å,[14] while $LaMg_2$ shows values around 7.40–7.42 Å.[15] In addition, La–Mg–RE systems are reported with lattice parameters between 7.38 and 7.46 Å.[16] These compounds demonstrate that similar rare-earth magnesium-based structures are stable.

## B. Hydrogen storage potential of $LaMgX_2H_n$ hydrides

Table II summarizes the calculated total energies and corresponding hydrogen formation energies (Ef) for the $LaMgX_2H_n$ systems (X = Zn, Cd, Hg). The formation energies were determined using the expression $E_F = E_{LaMgX2Hn} - E_{LaMgX2} - n/2E_{H_2}$.

As shown in the table, all $LaMgM_2H_n$ compounds exhibit significantly negative formation energies, indicating their thermodynamic stability with respect to decomposition into $LaMgM_2$ and $H_2$. Among the series, $LaMgZn_2H_x$ possesses the least negative Ef value (−175.63 eV), suggesting moderate hydrogen binding strength, which is advantageous for reversible hydrogen storage applications. In contrast, $LaMgCd_2H_x$ and $LaMgHg_2H_x$ demonstrate more negative formation energies (−284.93 and −328.51 eV, respectively), indicative of stronger metal–hydrogen interactions, which may require higher desorption temperatures. These computational results corroborate the hypothesis introduced at the outset of this study: the $LaMgM_2$-based hydrides are viable candidates for hydrogen storage.

## C. Elastic constants and related parameters

The elastic parameters were determined by solving the tensor matrix of nonlinear equations using the Charpin method.[20] In a

**TABLE II.** Calculated total and formation energies of $LaMgM_2H_n$ compounds (M = Zn, Cd, Hg).

| Compounds | Energy (eV) | Energy formation ($E_f$) |
|---|---|---|
| $LaMgZn_2H_x$ | −25 802.153 806 26 | −175.63 |
| $LaMgZn_2$ | −25 499.092 836 67 | |
| $LaMgCd_2H_x$ | −23 194.318 195 80 | −284.93 |
| $LaMgCd_2$ | −22 782.980 602 32 | |
| $LaMgHg_2H_x$ | −45 748.532 531 97 | −328.51 |
| $LaMgHg_2$ | −45 293.617 738 43 | |
| $H_2$ | −31.607 742 397 26 | |

crystal, where the elastic regime is linear, the relationship between the stresses σi and the corresponding strains εj conforms to Hooke's law,

$$\sigma_i = \sum_{j=1}^{6} C_{ij}\varepsilon_j, \tag{1}$$

where the coefficient $C_{ij}$ are the elastic stiffness constants of the crystal.

The deformation of a crystal by application of a deformation εj results in a stress, from which we obtain the elastic constants from Eq. (1),

$$\varepsilon_{11} = \varepsilon_1,\ \varepsilon_{22} = \varepsilon_2,\ \varepsilon_{33} = \varepsilon_3,\ \varepsilon_{12} = \varepsilon_{21} = \varepsilon_6/2,$$
$$\varepsilon_{13} = \varepsilon_{31} = \varepsilon_5/2,\ \varepsilon_{23} = \varepsilon_{32} = \varepsilon_4/2,$$

$$\varepsilon_{11} = \varepsilon_1,\ \varepsilon_{22} = \varepsilon_2,\ \varepsilon_{33} = 0,\ \varepsilon_{12} = \varepsilon_{21} = \varepsilon_6/2,\ \varepsilon_{13} = \varepsilon_{31} = 0,\ \varepsilon_{23} = \varepsilon_{32} = 0,$$

$$B_{VRH} = \frac{B_V + B_R}{2},\ G_{VRH} = \frac{G_V + G_R}{2}.$$

Young's modulus E and Poisson's ratio υ are obtained by $E = \frac{9BG}{3B+G}$ $\nu = \frac{3B-2G}{2(3B+G)}$.

For materials with cubic symmetry, the elasticity matrix simplifies to three essential constants: $C_{11}$, $C_{12}$, and $C_{44}$. As no experimental or theoretical elastic constants have been previously reported for these compounds, our results represent novel predictions. These critical parameters, which characterize the mechanical behavior of the materials, are compiled in Table III. The elastic constants $C_{11}$, $C_{12}$, and $C_{44}$ quantify the material's stiffness under different deformation modes. Among the three compounds, $LaMgZn_2$ exhibits the highest $C_{11}$ value, indicating superior resistance to deformation along crystallographic axes compared to its counterparts. The bulk modulus reflects a material's resistance to volumetric changes under applied pressure, while its pressure derivative describes how the bulk modulus itself varies with increasing pressure. $LaMgHg_2$ demonstrates a higher modulus of elasticity, signifying greater resistance to volumetric deformation compared to the other two intermetallic compounds.

The elastic constants and bulk modulus of $LaMgX_2$ (X = Cd, Zn, Hg) satisfy all mechanical stability criteria: $C_{11} + 2C_{12} > 0$, $C_{44} > 0$, $C_{11} > C_{12}$, and $C_{12} < B < C_{11}$, confirming that these intermetallic compounds are mechanically stable. Shear modulus quantifies a material's resistance to shape deformation under shear stress. Among the compounds, $LaMgZn_2$ demonstrates the highest shear modulus, indicating superior resistance to shear deformation. The B/G ratio serves as an indicator of material ductility, with B/G > 1.75 classifying a material as ductile, and B/G < 1.75 indicating brittleness. Our analysis shows that $LaMgHg_2$ possesses the highest B/G ratio, identifying it as the most ductile of the three compounds. For cubic crystals, positive Cauchy pressure (PC = $C_{12}$–$C_{44}$) indicates material ductility.[21–24] The calculated Cauchy pressures for $LaMgZn_2$, $LaMgCd_2$, and $LaMgHg_2$ are 3.66, 9.66, and 20.14 GPa, respectively, confirming their ductile nature and corroborating the B/G ratio results. Young's modulus and Poisson's ratio are fundamental parameters for evaluating polycrystalline material hardness. Young's modulus measures material stiffness, while Poisson's ratio represents the ratio between transverse strain (perpendicular to applied load) and axial strain (parallel to applied load) during stretching. These properties correlate with bulk and shear moduli through the following equations:[25]

$$B = \frac{C_{11} + 2C_{12}}{3}.$$

Young's modulus quantifies a material's resistance to elastic deformation under applied stress. With the highest E value, $LaMgZn_2$ demonstrates superior stiffness compared to the other two intermetallic compounds. Poisson's ratio characterizes the relationship between lateral and longitudinal strain during deformation. Higher values indicate greater material ductility. $LaMgHg_2$ exhibits the highest Poisson's ratio (ν), confirming its position as the most ductile of the three compounds. The Debye temperature reflects the crystal lattice's vibrational characteristics. $LaMgZn_2$ possesses the highest Debye temperature, indicating more pronounced thermal vibrations within its structure. From these analyses, we can conclude that $LaMgZn_2$ is the stiffest material with the greatest resistance to shear stress, while $LaMgHg_2$ emerges as the most ductile and least stiff compound. $LaMgCd_2$ occupies an intermediate position between these two extremes, with properties leaning more toward ductility than stiffness. The relatively modest elastic constants observed in $LaMgX_2$ (X = Cd, Zn, Hg) compounds can be attributed to their larger lattice spacings and consequently reduced Coulomb forces and hardness. The comparatively low values of bulk, shear, and Young's moduli in these double perovskites further substantiate their reduced hardness and rigidity. Numerous rare-earth intermetallic compounds containing magnesium and various transition metals have demonstrated bulk and shear moduli within similar ranges. For example, Mg–Zn–RE alloys have been reported to exhibit bulk modulus values between 45 and 55 GPa;[11] Mg–Cd–RE systems show moduli in the range of 40–50 GPa;[20] and Mg–Hg–RE alloys present values around 50–60 GPa.[21] These mechanical characteristics highlight the general mechanical robustness and stability of rare-earth-based intermetallic systems, Rare-earth intermetallic hydrides display Debye temperatures within close ranges. For

**TABLE III.** Elastic constants, bulk modulus, shear modulus, B/G ratio, Young's modulus, Poisson's ratio, and Debye temperature for $LaMgX_2$ (X = Zn, Cd, Hg).

| Compound | $C_{11}$ (GPa) | $C_{12}$ (GPa) | $C_{44}$ (GPa) | B (GPa) | G (GPa) | B/G | E (GPa) | υ | $\Theta_D$ (K) |
|---|---|---|---|---|---|---|---|---|---|
| $LaMgZn_2$ | 87.23 | 35.0 | 31.34 | 52.40 | 29.13 | 1.79 | 73.74 | 0.26 | 271.58 |
| $LaMgCd_2$ | 69.14 | 37.91 | 28.25 | 48.32 | 22.27 | 2.17 | 57.90 | 0.30 | 212.83 |
| $LaMgHg_2$ | 78.20 | 43.02 | 22.88 | 54.74 | 20.59 | 2.66 | 54.89 | 0.33 | 170.16 |

example, $LaNi_5$ alloys range between 260 and 280 K,[26] $LaMg_2$-type compounds between 200 and 220 K,[19] and La–Mg–RE systems from 160 to 190 K,[18] reflecting similar lattice dynamics and structural stability.

### D. Electronic properties

The electronic behavior of $LaMgX_2$ compounds (X = Zn, Cd, Hg) is best analyzed through their band structure and projected density of states (PDOS). The calculations were performed at 0 K, as is standard in density functional theory (DFT) calculations, as shown in Fig. 3. The band structure diagrams, located on the left side of each plot, display the energy of electronic states as a function of momentum (wave vector). In all three compounds, several energy bands clearly cross the Fermi level (set at 0 eV), indicating the presence of free electrons and confirming the metallic nature of these materials. The number and dispersion of bands vary across Zn, Cd, and Hg, reflecting subtle differences in atomic interactions and electron mobility. On the right, the PDOS curves break down the contributions of each element and orbital type (s, p, d) to the electronic structure. La–d orbitals contribute strongly near the Fermi level, while Zn, Cd, and Hg states dominate at lower energies. These PDOS profiles confirm orbital hybridization and support the band structure findings.

The comparison between GGA and GGA+U total DOS for $LaMgZn_2$, shown in Fig. 4, highlights the influence of on-site Coulomb interactions (U) on the electronic structure. In the GGA results, a pronounced peak appears slightly above the Fermi level (~2 eV), indicating a high density of unoccupied La-4f states. When applying the GGA+U correction, this peak is shifted slightly downward in energy, reflecting the repulsion introduced by the U term, which pushes the 4f states farther from the Fermi level. As a result, the density at the Fermi level decreases slightly, but remains nonzero preserving the metallic character of the compound. The shift in peak position also implies reduced hybridization between La and Cd orbitals. This adjustment corrects the common underestimation of f-state localization in standard GGA. Overall, GGA+U offers a more realistic picture of the electronic behavior of $LaMgCd_2$, especially regarding the role of La's localized 4f electrons.

### E. Thermal properties

#### *1. Debye vibrational energy*

The Debye model for the internal energy of a material predicts that the internal energy depends on the vibrational modes of the crystal. The phonons that contribute the most to the internal energy will occur at the maximum of the integrand in the Debye integral. The Debye model assumes that atoms in materials move in a collective fashion, described by quantized normal modes. The phonon modes exhibit uniform density throughout the reciprocal k-space. Figure 5 illustrates the temperature-dependent variations in Debye vibrational energy for $LaMgX_2$ (X = Zn, Cd and Hg) compounds. Debye vibrational energy represents the energy of atomic vibrations within the crystal lattice structure, which significantly influences thermal properties including specific heat and thermal conductivity. The Debye model specifically characterizes these collective atomic vibrations, termed "phonons." Beyond atomic mass considerations,

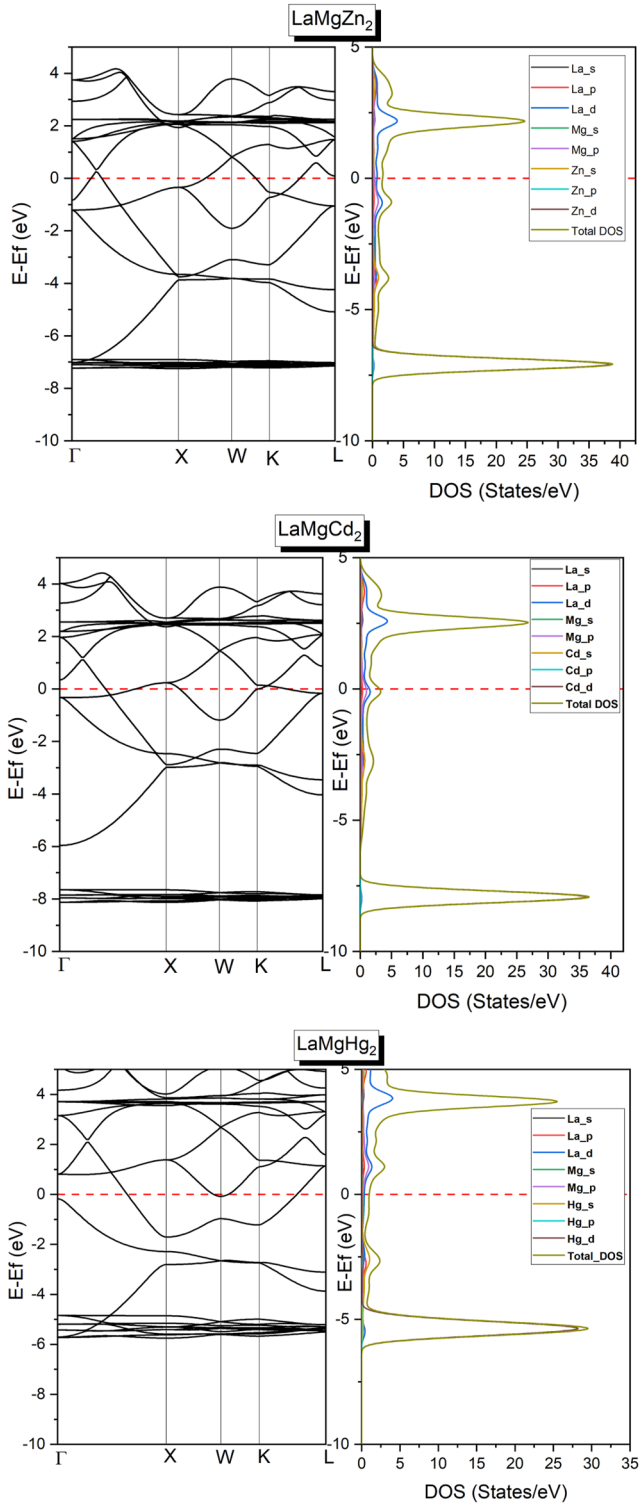


**FIG. 3.** Band structure of $LaMgZn_2$, $LaMgCd_2$, and $LaMgHg_2$ (left panel) and TDOS (right panel).

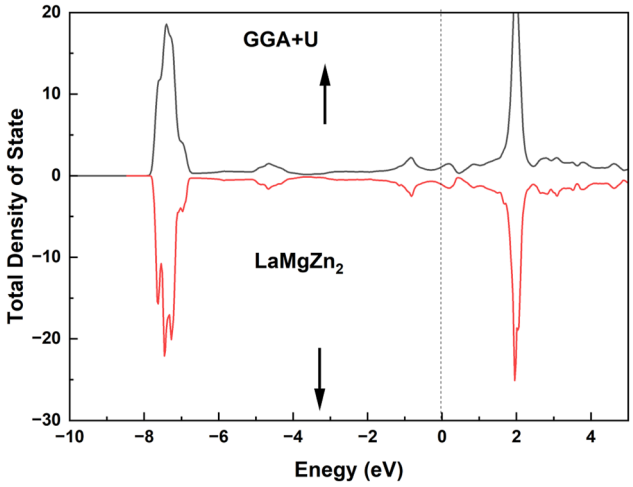


**FIG. 4.** Total density of the state of $LaMgZn_2$ using GGA+U approximation.

the vibrational behavior of these materials is substantially influenced by the strength of interatomic chemical bonds.

Stronger bonds require more energy to increase the vibrations, which influence how a material responds to changes in temperature. Near absolute zero (0 K), atomic vibrations are severely limited due to insufficient thermal energy, resulting in minimal Debye vibrational energy. As temperature rises, atoms acquire greater thermal energy, enabling more vigorous vibrations throughout the crystal lattice, which manifests as increased Debye vibrational energy.

We see that beyond 100, 150, and 200 K, the $LaMgHg_2$, $LaMgCd_2$, and $LaMgZn_2$ materials studied have negative vibrational free energy, which explains their thermodynamic stability. There is a phase transition at 100, 150, and 200 K for $LaMgHg_2$, $LaMgCd_2$, and $LaMgZn_2$ respectively.

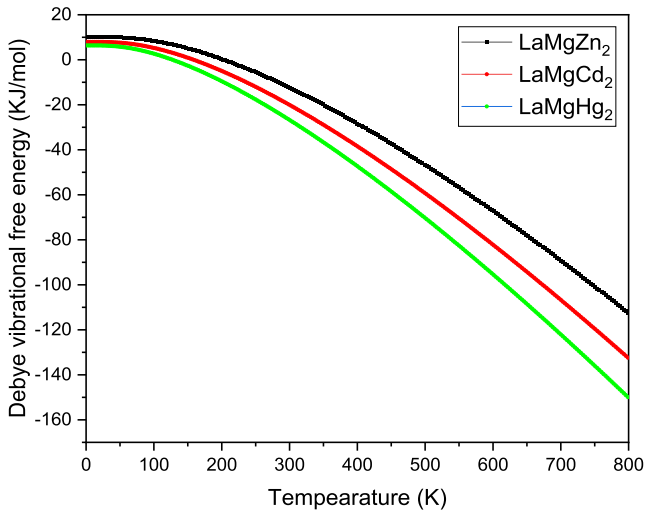


**FIG. 5.** Debye vibrational energy vs temperature for $LaMgX_2$ (X = Zn, Cd, and Hg).

### 2. Heat capacity at constant volume

The vibrational partition function for a system consisting of $N$ diatomic molecules is

$$Z_{vib} = \left(\frac{1}{\left(1 - e^{\frac{-\theta_{vib}}{T}}\right)}\right)^N,$$

where $Z_{vib}$ is the vibrational partition function of a diatomic system, $\theta_{vib}$ is the vibrational temperature, and T is the absolute temperature in Kelvin.

The vibrational contribution to the molar internal energy is

$$U_{vib} = k_B T^2 \left(\frac{\partial \ln Z_{vib}}{\partial T}\right) = \frac{N_{Av} k_B \theta_{vib}}{e^{\theta/T} - 1} = \frac{R\theta_{vib}}{e^{\theta/T} - 1}$$

where $k_B$ is the Boltzmann constant, $N_{AV}$ is Avogadro's number, R is the universal gas constant, and $\theta$ is the Debye temperature.

The vibrational contribution to molar heat capacity at constant volume is

$$C_{vib,V} = \left(\frac{\partial U_{vib}}{\partial T}\right)_V = R\left(\frac{\theta_{vib}}{T}\right)^2 \frac{e^{\theta_{vib}/T}}{\left(e^{\theta_{vib}/T} - 1\right)^2}.$$

Heat capacity at constant volume (CV) represents the ratio of change in internal energy to temperature variation, expressed as CV = $\partial$U/$\partial$T. Thermal energy is stored through the occupation of specific degrees of freedom within the material. CV quantifies the heat required to elevate a material's temperature while maintaining constant volume. Figure 6 illustrates the temperature dependence of constant volume heat capacity for $LaMgX_2$ (X = Zn, Cd, Hg) compounds. As temperature rises, the particles' kinetic energy increases, necessitating greater heat input to achieve further temperature elevation. At lower temperatures, particles occupy lower energy states. With increasing temperature, these particles access higher energy levels, resulting in a nearly linear increase in heat capacity.

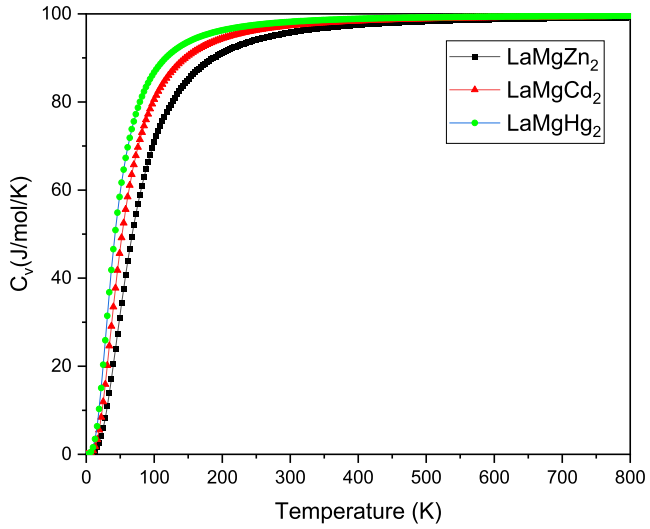


**FIG. 6.** Effect of temperature on constant volume heat capacity for $LaMgX_2$ (X = Zn, Cd, Hg).

Due to its lightest atomic mass composition, $LaMgZn_2$ exhibits more rapid lattice vibrations, resulting in elevated heat capacity at lower temperature ranges. Conversely, $LaMgHg_2$, containing the heaviest elements, demonstrates reduced vibrational frequencies, yielding lower heat capacity values. $LaMgCd_2$, with an atomic mass intermediate between the zinc and mercury variants, displays corresponding intermediate thermal behavior. As temperatures approach ~800 K, all three compounds reach thermal saturation, with heat capacities stabilizing as they approach their respective Debye limits. This represents the threshold at which all lattice vibrational modes become fully excited, resulting in a plateauing heat capacity. Comprehending the heat capacity characteristics of these compounds is essential for applications demanding thermal regulation and stability. Materials exhibiting higher heat capacities demonstrate superior thermal energy storage capabilities, rendering them particularly valuable in electronics industries and systems undergoing thermal transitions.

### 3. Entropy

Entropy quantifies system disorder or uncertainty by measuring the number of possible configurations that a system may adopt. When calculating the vibrational component of molar entropy, we must utilize a shifted energy scale, as including the zero-point contribution to the internal energy would result in an infinite value,

$$S_{vib,i} = R\left[\frac{\theta_{vib,i}}{T}\right]\left(\frac{\partial U_{vib}}{\partial T}\right)_V = R\left(\frac{\theta_{vib}}{T\left(e^{\theta_{vib}/T}-1\right)}\right) - \ln\left(e^{\theta_{vib}/T}-1\right).$$

As temperature increases, entropy rises predictably due to enhanced atomic and molecular motion, which amplifies system randomness. Figure 7 depicts the temperature-dependent thermodynamic entropy for $LaMgX_2$ (X = Zn, Cd, Hg) compounds. The data reveal a nearly linear relationship between entropy and temperature for all materials, indicating a consistent increase in disorder with rising temperature. $LaMgZn_2$ exhibits the lowest entropy values across all temperature ranges, suggesting that it possesses the most stable structure among the three compounds. The zinc atoms appear to constrain molecular motion more effectively than cadmium or mercury. Conversely, $LaMgHg_2$ demonstrates the highest entropy throughout the temperature spectrum, indicating that mercury atoms contribute most significantly to molecular disorder. This characteristic may result from mercury's greater atomic mass or specific atomic properties that enhance movement and disorder. $LaMgCd_2$ displays intermediate entropy values, positioned between $LaMgZn_2$ and $LaMgHg_2$. Its slightly elevated entropy compared to $LaMgZn_2$ likely stems from cadmium's larger atomic mass, which facilitates increased molecular motion.

At room temperature, entropy differences among the studied materials are minimal, with $LaMgHg_2$ exhibiting slightly higher values. Beyond 300 K, these differences become increasingly pronounced, as $LaMgHg_2$ demonstrates a steeper entropy increase, while $LaMgZn_2$ maintains the lowest entropy profile. Atomic mass significantly influences this behavior pattern. Conversely, materials with lower entropy, such as $LaMgZn_2$, demonstrate superior thermal stability, making them more suitable for environments requiring sustained performance at elevated temperatures.

## F. Thermoelectric properties

### 1. Seebeck coefficient

Figure 8 illustrates the variation of the Seebeck coefficient for $LaMgX_2$ compounds (where X = Cd, Hg, Zn) as a function of the chemical potential. The three compounds exhibit values near zero at the Fermi level, suggesting metallic behavior and weak thermoelectric properties in their undoped state. There is a clear correlation between the electronic structure calculations and the Seebeck characteristics, reinforcing the reliability of the predictions regarding the metallic nature of these compounds. At negative chemical potentials, a p-type behavior is observed, while at positive potentials, the behavior transitions to n-type with sharp negative peaks in Cd and

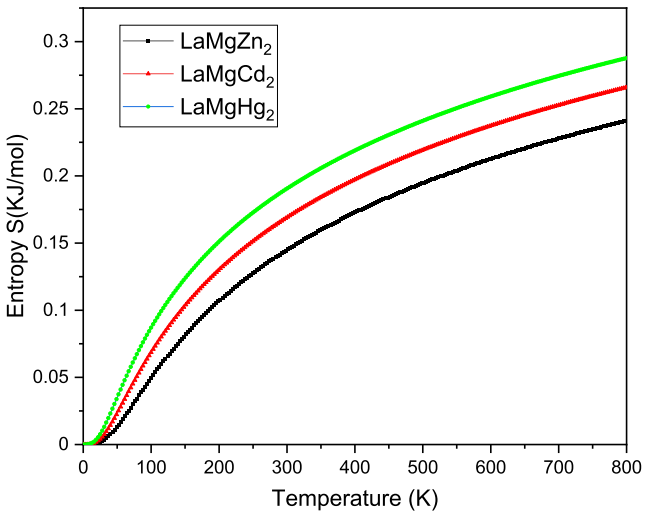


**FIG. 7.** Effect of temperature on thermodynamic entropy of $LaMgX_2$ (X = Zn, Cd, Hg).

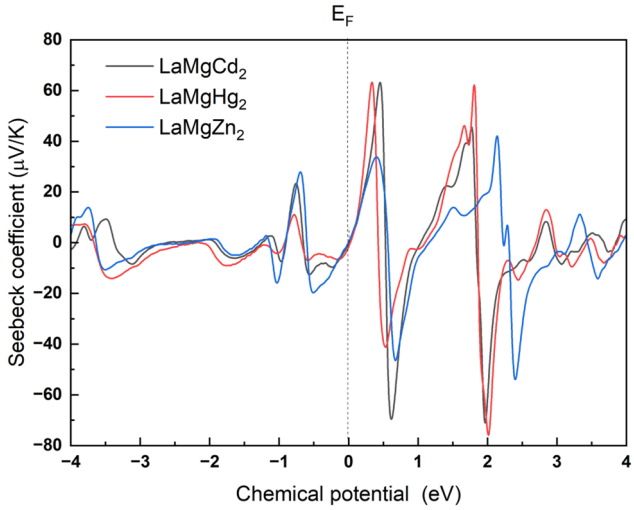


**FIG. 8.** Seebeck coefficient as a function of chemical potential at temperatures T = 300 K for $LaMgX_2$ X(Zn, Cd and Hg) using GGA approximation.

Hg. In contrast, the $LaMgZn_2$ compound demonstrates a more gradual and stable behavior, positioning it as a promising candidate for thermoelectric applications.

### 2. Electrical conductivity

Figure 9 represents the relationship between the electrical conductivity ($\sigma/\tau$) and chemical potential for three compounds: $LaMgCd_2$, $LaMgHg_2$, and $LaMgZn_2$. At the Fermi level ($E_F$), the compounds show moderate values ranging between 4 and 5.5 $(\Omega{\cdot}m{\cdot}K{\cdot}s)^{-1}{\cdot}10^{20}$. $LaMgHg_2$ exhibits a high value at 0 eV (~6.7) and a sharp decrease at 2 eV before reaching its highest value at 4 eV (~7). Meanwhile, $LaMgZn_2$ displays a distinctive peak at 1 eV (~6.5) that exceeds the other compounds in this region. $LaMgCd_2$ maintains moderate values throughout most of the range with a drop at 1 eV and fluctuations at high potentials. These variations reflect shifts in the electronic density of states of the materials and indicate the possibility of tuning their electronic properties by controlling the Fermi level, allowing for the selection of the appropriate compound for thermoelectric applications based on specific performance requirements.

### 3. Thermal conductivity

Figure 10 depicts the relationship between thermal conductivity ($K/\tau$) measured in W/m·K·s and chemical potential (eV) for three $LaMgX_2$ compounds: $LaMgCd_2$, $LaMgHg_2$, and $LaMgZn_2$. At the Fermi level (EF) marked by a vertical dotted line at 0 eV, the thermal conductivity values of all three compounds converge to approximately 3–4 W/m·K·s, suggesting similar thermal transport behavior at this critical energy level. All the compounds exhibit significant oscillations in thermal conductivity across the chemical potential range, with a notable sharp decrease around +2 eV, where $LaMgHg_2$ reaches its minimum value. In the negative chemical potential region (between −4 and 0 eV), $LaMgHg_2$ consistently shows lower thermal conductivity compared to the other compounds, while $LaMgCd_2$ demonstrates relatively stable behavior. At high positive chemical potential values (>+3 eV), $LaMgZn_2$ displays superior thermal conductivity, followed by $LaMgHg_2$ and then $LaMgCd_2$. The differences in thermal conductivity behavior can be attributed to the distinct electronic band structures of these compounds and the characteristic influence of Cd, Hg, and Zn elements on transport properties. These compounds show similar patterns, with peaks around +1 and +3 eV, indicating shared electronic structure characteristics despite their compositional differences.

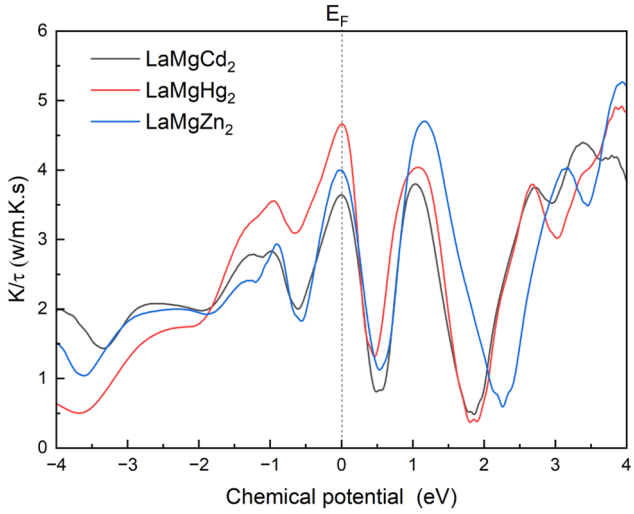


**FIG. 10.** Electronic thermal conductivity as a function of chemical potential at temperatures T = 300 for $LaMgX_2$ X(Zn, Cd and Hg) using GGA approximation.

### 4. Power factor

Figure 11 displays power factor curves as a function of chemical potential for three $LaMgX_2$ compounds: $LaMgCd_2$, $LaMgHg_2$, and $LaMgZn_2$. The power factor ($PF = S^2\sigma$) is crucial for evaluating thermoelectric performance, with higher values indicating

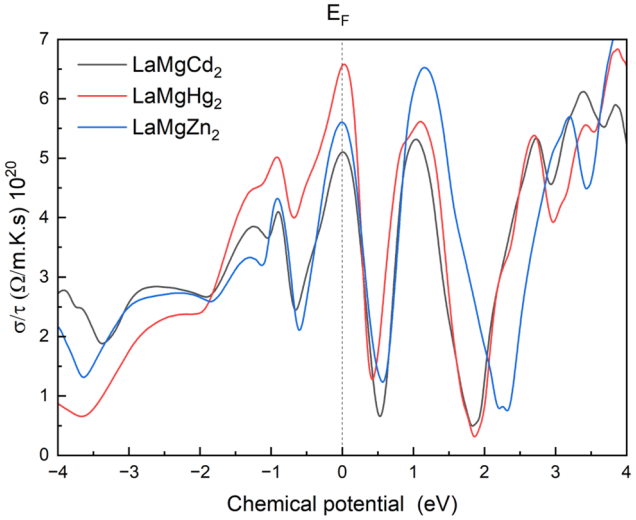


**FIG. 9.** Electrical conductivity as a function of chemical potential at temperatures T = 300 for $LaMgX_2$ X(Zn, Cd and Hg) using GGA approximation.

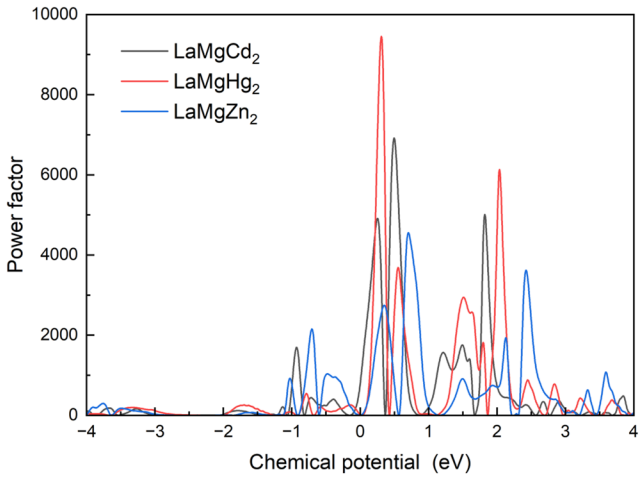


**FIG. 11.** Power factor as a function of chemical potential at temperatures T = 300 for $LaMgX_2$ X(Zn, Cd, and Hg) using GGA approximation.

better heat-to-electricity conversion efficiency. $LaMgHg_2$ demonstrates superior thermoelectric properties with the highest power factor peak of ~9500 near 0 eV (Fermi level), followed by $LaMgCd_2$ with a maximum value around 7000, also near 0 eV, and a secondary peak of about 5000 at 2 eV. $LaMgZn_2$ shows relatively lower values, with its primary peak reaching about 4500 at 0 eV and a secondary peak of 3500 at ~2.5 eV. All the compounds exhibit minimal power factor values in the negative chemical potential region (below −1 eV), indicating poor thermoelectric performance in this range. The sharp, narrow peaks rather than smooth curves suggest abrupt changes in electronic properties at specific energy levels and indicate that optimal thermoelectric performance occurs within very narrow chemical potential ranges, requiring precise doping control.

## IV. CONCLUSION

$LaMgX_2$(X = Cd, Zn, Hg) intermetallic alloys crystallize in the cubic structure, have potential practical experimental and materials optimization in hydrogen storage, and have lightweight structural applications and energy systems. $LaMgX_2$(X = Hg and Cd) alloys achieve minimum total energy at larger volume to achieve optimal stability, and the energy curve has a steep slope, hence their sensitivity to volume changes. The metallic bonding states between (La, Mg)-(Cd, Zn, Hg) and no zero TDOS at the Fermi level explain the metallic character of the studied alloys. The lightest (heaviest) mass and rapid lattice (slows) vibrations of $LaMgZn_2$ ($LaMgHg_2$) result in a higher (lower) heat capacity at lower temperatures. $LaMgHg_2$ ($LaMgZn_2$) material is less (more) stable with higher (lower) entropy at elevated temperatures, making $LaMgZn_2$more suitable for environments.

## ACKNOWLEDGMENTS

This work was funded by the Researchers Supporting (Project No. RSP2025R265), King Saud University, Riyadh, Saudi Arabia.

## AUTHOR DECLARATIONS

### Conflict of Interest

The authors have no conflicts to disclose.

### Author Contributions

**A. Benamrani**: Formal analysis (equal). **M. A. Ghebouli**: Investigation (equal). **B. Ghebouli**: Formal analysis (equal). **M. Fatmi**: Validation (equal). **Razan A. Alshgari**: Conceptualization (equal). **Saikh Mohammad**: Writing – original draft (equal). **Mika Sillanpää**: Project administration (equal).

## DATA AVAILABILITY

This manuscript has no associated data or the data will not be deposited. All the results presented in this paper can be reproduced with the information provided in the manuscript.

## REFERENCES

[1] J. Huot, M. L. Tremblay, and R. Schulz, "Synthesis of nanocrystalline hydrogen storage materials," J. Alloys Compd. **356–357**, 603–607 (2003).
[2] H. Okamoto, "Al-B (Aluminum-Boron)," J. Phase Equilib. Diffus. **27**, 195–196 (2006).
[3] B. L. Mordike and T. Ebert, "Magnesium: Properties applications potential," Mater. Sci. Eng.: A **302**(1), 37–45 (2001).
[4] E. Zhang, X. Wei, L. Yang, J. Xu, and C. Song, "Effect of Zn on the microstructure and mechanical properties of Mg–Si alloy," Mater. Sci. Eng.: A **527**(13–14), 3195–3199 (2010).
[5] S. Handschuh-Wang, T. Wang, T. Gancarz, X. Liu, B. Wang, B. He, M. D. Dickey, G. W. Wimmer, and F. J. Stadler, "The liquid metal age: A transition from Hg to Ga," Adv. Mater. **36**(45), 2408466 (2024).
[6] J. F. Lutsko, "Generalized expressions for the calculation of elastic constants by computer simulation," J. Appl. Phys. **65**(8), 2991 (1989).
[7] A. Züttel, S. Rentsch, P. Fischer, P. Wenger, P. H. Sudan, P. Mauron, and C. J. Emmenegger, "Hydrogen storage properties of $LiBH_4$," J. Alloys Compd. **356–357**, 515–520 (2003).
[8] M. Sato and V. A. Yartys, "Thermodynamic properties of the $NdNi_5Sn$-H system," J. Alloys Compd. **379**(1–2), 171–175 (2004).
[9] K. Bouferrache, M. A. Ghebouli, Y. Slimani, B. Ghebouli, M. Fatmi, T. Chihi, M. A. Habila, N. H. Alotaibi, and M. Sillanpaa, "Effect of functional on structural, elastic stability, optoelectronic and thermoelectric characteristics of semiconducting $MgX_2Se_4$ (X = Lu, Y) spinels," Bull. Mater. Sci. **47**(2), 102 (2024).
[10] B. Ghebouli, M. A. Ghebouli, M. Fatmi, and S. I. Ahmed, "First-principles study of structural, elastic, electronic and lattice dynamic properties of $As_xP_yN_{1-x-y}B$ quaternary alloys," Comput. Mater. Sci. **48**(1), 94–100 (2010).
[11] M. A. Ghebouli, K. Bouferrache, F. K. Alanazi, B. Ghebouli, and M. Fatmi, "Stability, mechanical, optoelectronic and thermoelectric behaviors of inorganic metal halide double perovskites (Cs, K, Rb)SnCl: Promising green energy alternatives," Solid State Commun. **397**, 115831 (2025).
[12] M. A. Ghebouli, B. Ghebouli, M. Fatmi, and T. Chihi, "Study of the structural, elastic, electronic and optical properties of the ternary acetylides $A_2MC_2$ (A = Na, K) and (M = Pb, Pt)," J. Korean Phys. Soc. **75**, 678–684 (2019).
[13] A. Dal Corso, "Elastic constants of beryllium: A first-principles investigation," J. Phys.: Condens. Matter **28**(7), 075401 (2016).
[14] J. Dai, K. Li, W. D. Han, Y. H. Li, Y. F. Li, W. L. Yin, and Z. Hu, "First-principles investigation on the structural, electronic, mechanical and thermodynamic properties of binary phase in Mg-1Si-3RE(RE = La, Ce) alloys," Mater. Today Commun. **26**, 101738 (2021).
[15] L. Bai, Q. Li, S. A. Corr, Y. Meng, C. Park, S. V. Sinogeikin, C. Ko *et al.*, "Pressure-induced phase transitions and metallization in $VO_2$," Phys. Rev. B **91**(10), 104110 (2015).
[16] K. Govaerts, K. Park, C. De Beule, B. Partoens, and D. Lamoen, "Erratum: Effect of Bi bilayers on the topological states of $Bi_2Se_3$: A first-principles study [Phys. Rev. B 90, 155124 (2014)]," Phys. Rev. B **91**(15), 159905 (2015).
[17] H. Arı and Z. Büyükmumcu, "Comparison of DFT functionals for prediction of band gap of conjugated polymers and effect of HF exchange term percentage and basis set on the performance," Comput. Mater. Sci. **138**, 70–76 (2017).
[18] X. Jiang, X. Chen, Q. Li, D. Wang, and Z. Wu, "Application and research progress of first principles calculation in magnesium alloys," Mater. Today Commun. **41**, 110317 (2024).
[19] G. Chen and P. Zhang, "First-principles study of electronic structures, elastic properties and thermodynamics of the binary intermetallics in Mg–Zn–Re–Zr alloy," Def. Technol. **9**(3), 131–139 (2013).
[20] S. A. Mir, A. Q. Seh, and D. C. Gupta, "New ferromagnetic half-metallic perovskites for spintronic applications: $BaMO_3$ (M = Mg and Ca)," RSC Adv. **10**(60), 36241–36252 (2020).
[21] C. Yang, Y. Duan, J. Yu, M. Peng, S. Zheng, and M. Li, "Elastic anisotropy and thermal properties of M-B-N (M = Al, Ga) systems using first-principles calculations," Vacuum **207**, 111626 (2023).
[22] H. Bai, Y. Duan, H. Qi, M. Peng, M. Li, and S. Zheng, "Anisotropic elastic and thermal properties and damage tolerance of CrH: A first-principles calculation," Vacuum **222**, 112962 (2024).

[23]X. Lei, A. Yang, L. Zhou, Y. Duan, L. Ma, M. Li, and M. Peng, "First-principles calculations of phase stability, electronic structure, mechanical properties and thermal conductivities of $TMH_2$ (TM=V, Nb, Ta) metal hydrides," Mater. Today Commun. **41**, 110549 (2024).
[24]Y. Wu, L. Ma, X. Zhou, Y. Duan, L. Shen, and M. Peng, "Insights to electronic structures, elastic properties, fracture toughness, and thermal properties of $M_{23}C_6$ carbides," Int. J. Refract. Met. Hard Mater. **109**, 105985 (2022).
[25]M. Hamici, F. K. Alanazi, T. Chihi, M. Fatmi, and M. A. Ghebouli, "Optical, structural, electronic, and population analysis of $WO_3$ – $Bi_2O_3$ system for emerging and electrical applications," J. Indian Chem. Soc. **102**, 101729 (2025).
[26]M. W. Barsoum, T. El-Raghy, W. D. Porter, H. Wang, J. C. Ho, and S. Chakraborty, "Thermal properties of $Nb_2SnC$," J. Appl. Phys. **88**(11), 6313–6316 (2000).